

# Does Monocular Depth Estimation Provide Better Pre-training than Classification for Semantic Segmentation?

Dong Lao\*, Alex Wong\*, and Stefano Soatto

UCLA Vision Lab  
{lao, alexw, soatto}@cs.ucla.edu

**Abstract.** Training a deep neural network for semantic segmentation is labor intensive, so it is common to pre-train it for a different task, and then fine-tune it with a small annotated dataset. State-of-the-art methods use image classification for pre-training, which introduces uncontrolled biases. We test the hypothesis that depth estimation from unlabeled videos may provide better pre-training. Despite the absence of any semantic information, we argue that estimating scene geometry is closer to the task of semantic segmentation than classifying whole images into semantic classes. Since analytical validation is intractable, we test the hypothesis empirically by introducing a pre-training scheme that yields an improvement of 5.7% mIoU and 4.1% pixel accuracy over classification-based pre-training. While annotation is not needed for pre-training, it is needed for testing the hypothesis. We use the KITTI (outdoor) and NYU-V2 (indoor) benchmarks to that end, and provide an extensive discussion of the benefits and limitations of the proposed scheme in relation to existing unsupervised, self-supervised, and semi-supervised pre-training protocols.

**Keywords:** network pre-training, semantic segmentation, unsupervised depth estimation

## 1 Introduction

Semantic segmentation partitions an image into “objects” implicitly defined as regions of its domain with an associated label chosen among a finite set of classes, typically by human annotators. Variants of semantic segmentation include the case where regions corresponding to each class are further subdivided into connected components (semantic instance segmentation), or where relations among different regions are also assigned labels (image parsing). We focus on the simplest case, corresponding to pixel-level image classification.

Training deep neural networks (DNNs) for semantic segmentation in a supervised fashion is extremely costly, as they require massive datasets and pixel-level annotation is laborious. It is therefore common practice to pre-train a “backbone” (representation) using either a different task, for instance image-level classification, or using synthetic data. Fine-tuning can then be performed using a small annotated dataset. But domain adaptation from synthetic data remains an open challenge [15,34,41,33]. Thus far, state-of-the-art methods pre-train the backbone using ImageNet classification [7,25,20] which introduces biases whose effects on semantic segmentation are only beginning to be investigated [14,45]. Since each image is only assigned one “true” label if, say, an image displays a cow and a barn but is labeled as “cow,” the training process informs the model that images of barns should be associated to the label “cow” even if no cow is visible. This accidental bias may be beneficial, since objects are in the scene not the image: The presence of a barn indeed suggests a cow may be nearby. But the bias is uncontrolled and highly dataset-dependent. Moreover, training sets for image classification come from photo collections where users tend to assign the label of objects that appear in a somewhat “canonical” pose. For example, an image with a cow facing the camera and a barn in the background is typically labeled as “cow,” whereas an image of the same scene with the cow seen from behind would likely be labeled as “barn.”

**Main hypothesis.** The biases described arise from the strong semantic priors imposed by human annotators, who associate labels to objects in a *scene*, yet assign them to pixels in an image. *We therefore hypothesize*

---

\*: contributed equally.

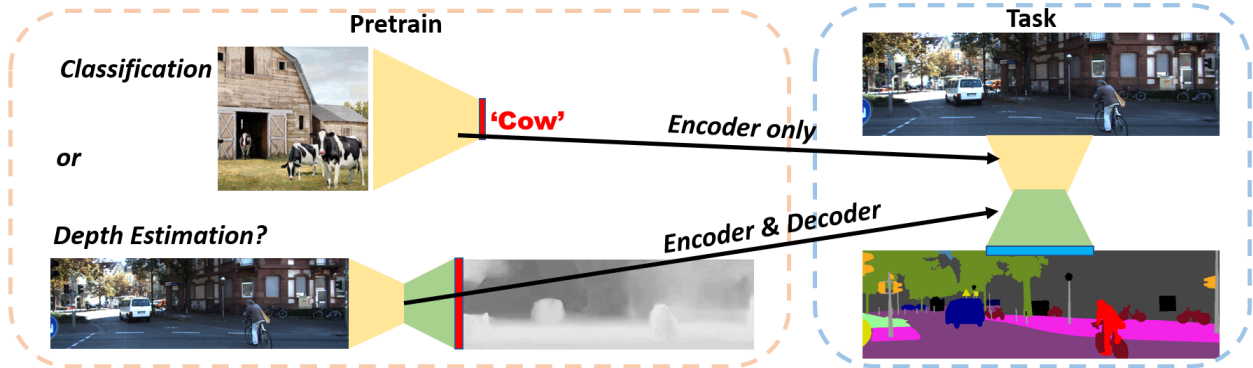


**Fig. 1.** Image classification introduces uncontrolled biases when used to pre-train semantic segmentation networks, where one requires an additional decoder. By replacing classification with depth estimation, we remove any semantic bias, eliminate the need for human annotation, and can easily adapt the pre-training dataset to the domain of interest. The key question is whether such a process can improve performance and reduce dependency of annotated datasets in fine-tuning for semantic segmentation.

that removing semantics altogether from the pre-training process may eliminate these biases and improve the performance of semantic segmentation downstream. The goal of this paper is to test this hypothesis. Our findings are discussed next, and their relevance in relation to prior work in the next section.

**Methods.** We first formalize the main hypothesis in Sect. 3.1 and conclude that it cannot be validated analytically without knowledge of the joint distribution of test images and labels. We therefore use the formalization to guide an empirical protocol to test the hypothesis empirically in Sect. 3.2. There, we use a baseline method for monocular depth prediction, Monodepth2 [12], trained to minimize the reprojection error with an edge-aware regularizer motivated by [19,18] and no other supervision. We then change the last layer of the resulting network and fine-tune it for semantic segmentation. For the alternate hypothesis, we pre-train Monodepth2 for image classification, both from scratch and after ImageNet pre-training, and then replicate the leading method by adding a DeepLab [7] decoder, and again fine-tune it for semantic segmentation. The hypothesis is then tested using the unlabeled KITTI (outdoor) and NYU-V2 (indoor) datasets for pre-training, and the held-out KITTI and NYU-V2 semantic dataset annotated for semantic segmentation, with part of its images used for fine-tuning, and the rest sequestered for testing. All models are trained for the same number of epochs according to the protocol in Fig. 2.

**Findings.** Using the protocol defined above, we find that pre-training for depth estimation (referred to as “ours”) does indeed improve the performance of semantic segmentation compared with pre-training for classification, on average by 5.7% mIoU and 4.1% pixel accuracy (Tab. 1). More specifically, when fine-tuning the full model, ours outperforms ImageNet pre-training by 6.3%. Freezing the encoder, ImageNet pre-training fails to yield a viable backbone, resulting in performance worse than random initialization even after extensive hyperparameter optimization. To test the limits of small fine-tuning datasets, we run experiments ranging from 128 to only 8 fully annotated images. Again, our method consistently outperforms pre-training for classification (Fig. 4). One unexpected twist, however, is that using ImageNet pre-training prior to pre-training for depth estimation improves the effectiveness of the latter in downstream semantic segmentation, compared to pre-training from scratch. To control the effect of our choice of architecture, we used our pre-trained encoder to initialize a standard semantic segmentation network [7], and observe that it still improves mIoU marginally. We observed similar findings for experiments on NYU-V2.

Since depth is inferred using a prediction criterion, albeit with respect to a structured deformation induced by a latent depth map, it is important to test the hypothesis against minimizing the prediction error with respect to an unstructured displacement field, or optical flow. The latter has two degrees of freedom

(displacement) per pixel, whereas the former has one. Somewhat surprisingly, not only does pre-training for depth estimation outperform unstructured video prediction, but the latter is often worse than random initialization (Fig. 11).

## 2 Related Work

The goal of pre-training is to learn a generic representation (a function of the test data) that is maximally informative (sufficient) for downstream tasks while providing some kind of complexity advantage [30]. Without the latter, the problem is trivial since any invertible function of the data is sufficient. In our case, we seek complexity reduction in the form of reduced need for annotated data. ImageNet pre-training achieves this by classifying the entire image with a single label. We are instead interested in fully unsupervised pre-training. Since semantic inference necessarily requires induction (Sect. 5), the pre-training task cannot be semantic. The recent literature comprises a large variety of “self-supervised” methods. These are reconstruction, prediction or classification tasks where the data is corrupted by some kind of hand-designed nuisance transformation. Such transformations can operate on the image domain, such as planar groups (rotation, translation, scaling, skew, reflection), or on its range (contrast changes, colorization). The goal of self-supervised learning is then to map each image and its transformed versions either to a class (contrastive learning [10,9]), or to a canonical (uncorrupted) image [5].

For the case of group transformations, whether acting on the domain or range of the images, the resulting representations approximate an invariant to that group. However, the maximal invariant to domain and range image transformations, induced by changes of viewpoint and illumination, could in theory be computed analytically, without the need for induction nor for learning [31]. The group organizes the data space into orbits, and the quotient is the maximal invariant. Contrastive learning, that can be thought of as a form of data augmentation [35,47], attempts to map transformed data to the base of the orbit space, and to keep orbits separated. Occlusions play a special role, in that they do not form a group; maximal invariants are trivial since all orbits collapse to a single point. Indeed, reconstructing occluded data has been an effective pre-training tool both in large language models [4] as well as in images [8,42]. While these forms of pre-training are often labeled as “task agnostic,” the task plays a key role in the choice of transformations used for data augmentation or to fashion the so-called “pretext task.” For instance, using contrast transformations as nuisances in pre-training prevents use of the trained model for X-ray image classification, where the gray-scale value is informative of the tissue class.

It is therefore essential to choose pre-training tasks that are in some sense “close” to the target task(s) downstream [1,46]. At the very least, they must share the same nuisance variability. At best, they share the same hypothesis space. Thus, it may seem odd to choose a geometric task, where the hypothesis space is depth, to pre-train for a semantic task, where the hypothesis space is a discrete set of labels with no topology. However, due to the statistics of range images [18] and their similarity to the statistics of natural images [19], this is not as odd as it may seem: A range map is a piecewise smooth function defined on the image domain, whereas a segmentation map is a piecewise constant function where the levels are mapped to arbitrary labels. As a result, the decoder for depth estimation can be easily modified for semantic segmentation.

Rather than designing pretext tasks, temporal continuity provides one bit of critical supervision, which makes prediction a natural task: Future images are, by definition, affected by all relevant nuisance variability. At the same time, if we are interested in a particular task that does not require pixel-level prediction, we can design the discrepancy measure to penalize not pixel value differences, but rather any function of those, for instance a contrast invariant such as the gradient orientation [27]. We adopt this vantage point and train a depth estimation network with a predictive task, specifically the reprojection error. Details are in Sect. 4.1 and a critical discussion of this choice, specifically on the representational power of deterministic predictors, is in Sect. 5.

Some methods for monocular depth estimation do use supervision, whether through additional sensors [39], or using synthetic data [37,26]. Some are obtained through learned regularizers from a sparse “seed” [38], others yet use ImageNet pre-training, just because it is available [12]. Our conclusions are agnostic to how depth estimation models are trained. Even if it were to involve supervision, the important aspect of using

depth estimation is that, unlike classification, *inductive bias is not required*. This was made clear already in the Sixties by the work of Julesz [23] on depth an motion [22]: Random dot stereograms allows depth estimation without any photometric cues that can be associated to semantics or interpretation. Binocular disparity can be obtained by minimizing the re-projection error, with generic priors and without the need for any inductive prior from images of scenes other than the one in question. This is a qualitative and fundamental difference on which we elaborate in Sect. 5. There are also works using unsupervised depth estimation for semantic segmentation [17,16]. While relevant as prior art, they use depth as supervision, for sampling and data augmentation, whereas we use it as a criterion for generic pre-training.

### 3 Pre-training for Semantic Segmentation

We first formalize the main hypothesis, then show that it cannot be tested analytically absent knowledge of the joint distribution of future data. We then use the formalization to guide the empirical protocol used in the next section.

#### 3.1 Formalization

Let  $x : D \subset \mathbb{R}^2 \rightarrow \{0, \dots, 255\}$  be a gray-scale image, where the domain  $D$  is quantized into a lattice,  $z : D \rightarrow \{1, \dots, Z\}$  a depth map with  $Z$  depth or disparity levels, and  $y : D \rightarrow \{1, \dots, K\}$  a semantic segmentation map. In coordinates, each pixel in the lattice,  $(i, j) \in \{1, \dots, N\} \times \{1, \dots, M\}$  is mapped to a gray-scale level by  $x(i, j)$ , a depth by  $z(i, j)$ , and a label by  $y(i, j)$ . Despite the discrete nature of the data and the hypothesis space, we relax them to the continuum by considering the vectors  $\mathbf{x} \in \mathbb{R}^{NM}$ ,  $\mathbf{y} \in \mathbb{R}^{NMK}$  and  $\mathbf{z} \in \mathbb{R}^{NMZ}$ . With a slight abuse of notation, we indicate with  $y \in \{1, \dots, K\}$  a single label and  $\bar{y} \in \mathbb{R}^K$  its embedding, often restricted to a binary unit-norm vector (one-hot encoding). Whether  $y$  is understood as a map (a label per pixel) or as a label should be clear from the context.

Now, consider two pre-training datasets: One  $\mathcal{D}_z = \{\mathbf{x}_t^i\}_{i,t=1}^{V,T_i}$  comprised of  $V$  video sequences each of length  $T_i$ . The other  $\mathcal{D}_y = \{\mathbf{x}^i, y^i\}_{i=1}^L$  comprised of  $L$  pairs of images and their corresponding label, typically provided by human annotators. Pre-training for depth estimation yields a map  $\phi_w : \mathbf{x} \mapsto \mathbf{z}$ , parametrized by weights  $w$ , via

$$\mathbf{z} = \phi_w(\mathbf{x}|\mathcal{D}_z) = \arg \min_{w, g_t} \sum_{i,j,n,t} = \ell(x_{t+1}^n(i, j), \hat{x}_t^n(i, j)) \quad (1)$$

where

$$\hat{x}(i, j) = x \circ \pi_{g,z}^{-1}(i, j) \quad (2)$$

is the *warping* of an image  $x$  onto the image plane of another camera related to it by a change of pose  $g \in SE(3)$ , through the depth map  $z$ , via a *reprojection map*  $\pi^{-1}$

$$\pi^{-1}(i, j) = K_+ \pi(R_t K^{-1}[i, j, 1]^T z(i, j) + T_t) \quad (3)$$

that embeds a pixel  $(i, j)$  in homogeneous coordinates and places it in the camera reference frame through a calibration matrix  $K$ , back-projects it onto the scene by multiplying it by the depth

$$z(i, j) = \phi_w(x(i, j)|\mathcal{D}_z) \quad (4)$$

and then transforming it to the reference frame of another camera with a rigid motion  $g = (R, T)$ , where the rotation matrix  $R \in SO(3)$  and the translation vector  $T \in \mathbb{R}^3$  transform the coordinates of spatial points  $P \in \mathbb{R}^3$  via  $P \mapsto RP + T$ . Here  $\pi$  is a canonical perspective projection  $\pi(P) = [P(1), P(2)]/P(3)$  and the calibration map  $K_+$  incorporates quantization into the lattice. Here, we assume that the intrinsic calibration matrix  $K$  is known, otherwise it can be included among nuisance variables in the optimization along with the inter-frame pose  $g_t$  when minimizing the reprojection error  $\ell$  in (1).

Note that the reprojection error could be minimized with respect to  $w$ , which is shared among all images and yields a depth map through  $z_t = \phi_w(x_t|\mathcal{D}_z)$ , or directly with respect to  $z_t$  in (3), which does not require



any induction. Since the purpose of pre-training is to capture the inductive bias we obviously adopt the former, and discuss this issue in more detail in Sect. 5.

Pre-training for classification yields a different map  $\phi_w : \mathbf{x} \mapsto y$ , parametrized by different weights  $w'$ , obtained via

$$y = \phi_{w'} = \arg \min_w \sum_{n,t=1} -\log p_w(y_t^n | \mathbf{x}_t^n) \quad (5)$$

where

$$p_w(y|\mathbf{x}) \propto \exp(\langle \bar{y}, \phi_w(\mathbf{x}; \mathcal{D}_y) \rangle) \quad (6)$$

and  $\bar{y}$  is the one-hot encoding of the ground truth label  $y$ . Note that, in this case, labels can only be predicted through the training set  $\mathcal{D}_y$  via the inductive map  $\hat{y} = \phi_{w'}(\mathbf{x}|\mathcal{D}_y)$  since the data  $\mathbf{x}$  does not contain any information about the label without access to the dataset  $\mathcal{D}_y$ .

Thus, pre-training for depth estimation yields a representation of the data  $\mathbf{x}$  given by  $\phi_w(\mathbf{x}|\mathcal{D}_z) \in \mathbb{R}^{ZNM}$ , the depth hypothesis space, whereas pre-training for classification yields a representation  $\phi_{w'}(\mathbf{x}|\mathcal{D}_y) \in \mathbb{R}^K$ , the classification hypothesis space; the goal is to use these representations, or embeddings, as encodings of the data to then learn a semantic segmentation map. In practice, the representations above are implemented by deep neural networks, that can be truncated at intermediate layers thus providing embedding spaces larger than the respective hypothesis spaces. We overload the notation and refer to the encoding as  $\mathbf{z} = \phi_w(\mathbf{x})$  for both depth estimation and classification. The goal of semantic segmentation is then to learn a parametrized map  $\psi_{w''} : \mathbf{z} \mapsto \mathbf{y}$  using a small but fully supervised dataset  $\mathcal{D}_s = \{\mathbf{x}^n, \mathbf{y}^n\}_{n=1}^N$ , by minimizing some loss function or (pseudo-)distance in the hypothesis space  $d(\mathbf{y}, \hat{\mathbf{y}})$ , where

$$w'' = \arg \min_w \sum_{n=1}^N d(\mathbf{y}^n, \psi_w(\mathbf{x}^n)) \quad (7)$$

plus customary regularizers. In the aggregate, we have a Markov chain:

$$\mathbf{x} \longrightarrow \mathbf{z} = \phi_w(\mathbf{x}) \longrightarrow \mathbf{y} = \psi_{w''}(\mathbf{z}) = \psi_{w''} \circ \phi_w(\mathbf{x}) \quad (8)$$

for depth estimation, and

$$\mathbf{x} \longrightarrow \bar{y} = \phi_{w'}(\mathbf{x}) \longrightarrow \mathbf{y} = \psi_{w''} \circ \phi_{w'}(\mathbf{x}) \quad (9)$$

for classification. A representation obtained through a Markov chain is optimal (minimal sufficient) only if the intermediate variable  $\mathbf{z}$  or  $\bar{y}$  reduces the Information Bottleneck [32] to zero. In general, there is information loss, so we **formalize the question** set forth in the title of the paper as whether the two Information Bottleneck Lagrangians satisfy the following:

$$H(\mathbf{y}|\mathbf{z}) + \beta I(\mathbf{z}; \mathbf{x}) \stackrel{?}{\leq} H(\mathbf{y}|\bar{y}) + \beta' I(\bar{y}; \mathbf{x}) \quad (10)$$

where  $\beta$  and  $\beta'$  are hyperparameters that can be optimized as part of the training process, and  $I, H$  denotes the (Shannon) Mutual Information and cross-entropy respectively. If the above is satisfied, then pre-training for depth estimation is better than pre-training for image classification. It would be ideal if this question could be settled analytically. Unfortunately, this is not possible, but the formalization above suggests empirical protocols to settle it empirically.

### 3.2 Analytical decidability and empirical set-up

Unfortunately, the Information Bottleneck Lagrangian cannot be computed because we do not have access to the analytical form of the joint distributions of the variables  $(\mathbf{x}, \mathbf{z})$ ,  $(\mathbf{z}, \mathbf{y})$  and  $(\mathbf{x}, \bar{y})$ ,  $(\bar{y}, \mathbf{y})$ . Even defining, let alone computing, the Shannon Information for random variables that are deterministic maps  $\phi(\cdot)$  of variables  $\mathbf{z}$  defined in the continuum is non-trivial [2]. It is possible, however, to bound the Information Bottleneck, which is not computable, with the *Information Lagrangian* [3], which only depends on the datasets  $\mathcal{D}_y, \mathcal{D}_z$

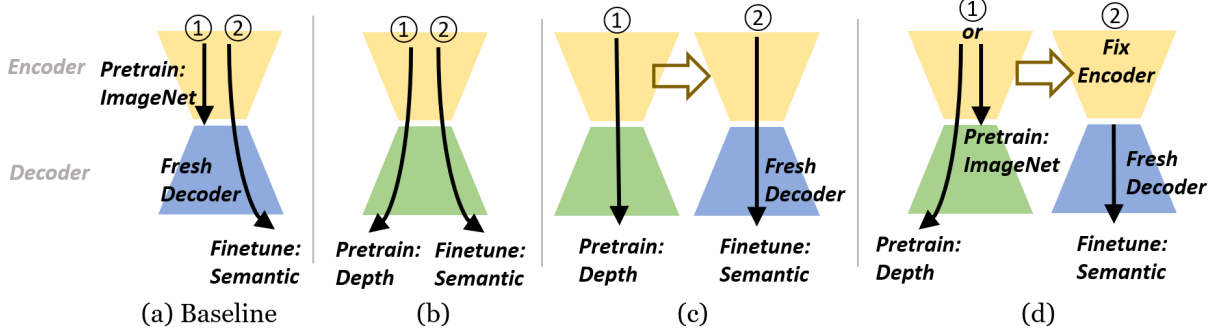


**Fig. 2. Diagram for different pre-training and fine-tuning setups.** (a) Common practice: pre-train encoder on ImageNet, attach to a decoder (e.g DeepLab), fine-tune the whole network for semantic segmentation. (b) Our best practice: pre-train by monocular depth, fine-tune both encoder and decoder for semantic segmentation. (c) Cross architecture: for fair comparison with common practice, we pre-train by depth, replace the decoder by DeepLab and fine-tune. (d) To test the quality of pre-trained encoders, we fix the encoders and fine-tune decoders only.

and  $\mathcal{D}_s$ . However, the bound depends on constants that are functions of the complexity of the datasets, which are different for different tasks, which would render them useless in answering the question in (10).

The bottom line is that, unless the analytical form of the densities at play is known, or strong additional assumptions are imposed, the question cannot be settled analytically. Instead, we must consider proxies using the validation error (or average test error) as a measure of residual information:

$$L_z(w''|w) = \sum_{\mathbf{z}^n = \phi_w(\mathbf{x}^n)} -\log p_{w''}(\mathbf{y}^n|\mathbf{z}^n) \simeq H(\mathbf{y}|\mathbf{z}) \quad (11)$$

for pre-training using depth estimation, and

$$L_y(w''|w') = \sum_{\bar{\mathbf{y}}^n = \phi_{w'}(\mathbf{x}^n)} -\log p_{w''}(\mathbf{y}^n|\bar{\mathbf{y}}^n) \simeq H(\mathbf{y}|\bar{\mathbf{y}}) \quad (12)$$

for pre-training using image classification. The complexity terms  $I(\mathbf{z}; \mathbf{x})$  and  $I(\bar{\mathbf{y}}; \mathbf{x})$  are minimized implicitly by the capacity control mechanisms in the architecture (*i.e.*, the maps  $\phi_w(\cdot|\mathcal{D}_z)$  and  $\phi_{w'}(\cdot|\mathcal{D}_y)$ ), for instance pooling; in the regularizers, for instance weight decay and data augmentation [2]; and in the optimization, for instance stochastic gradient descent [6]. The losses above are computed by summing over the samples in the validation set  $\mathcal{D}_s = \{\mathbf{x}^n, \mathbf{y}^n\}$ .

Now, the two losses above can be optimized with respect to  $w''$  using a fine-tuning dataset, yielding a comparison of the raw pre-trained back-bone (encoder), or they can be optimized with respect to *both*  $w''$  and  $w$  (for depth estimation) or  $w'$  (for image classification). Finally, all four resulting models can be compared with one obtained by training from scratch by optimizing a generic architecture with respect to  $w''$  alone. These settings are visualized in Fig. 2.

The corresponding experiments, choice of pre-training, fine-tuning, and validation datasets are discussed in more detail in the next section.

## 4 Experiments

### 4.1 Implementations

We use Monodepth2 [12] for unsupervised depth estimation. Monodepth2 consists of a pose estimation network and a monocular depth estimation network. The depth network adopts a standard encoder-decoder architecture, where the encoder supports generic backbones including ResNet. Monodepth2 is trained by

	Fine-tune All						Freeze Encoder			
	ResNet18		ResNet50		DeepLabV3 <sup>†</sup>		ResNet18		ResNet50	
Pre-training	mIoU	P.Acc	mIoU	P.Acc	mIoU	P.Acc	mIoU	P.Acc	mIoU	P.Acc
None	41.35	70.75	44.66	73.37	21.93	52.32	41.24	70.52	37.72	67.38
ImageNet	45.15	72.39	44.65	73.06	<b>43.39</b>	<b>72.66</b>	<b>33.33</b>	<b>65.34</b>	<b>32.03</b>	<b>62.53</b>
Depth	46.00	72.43	49.90	76.28	43.43	71.34	43.02	72.38	45.79	<b>74.71</b>
Depth-IN	<b>50.20</b>	<b>76.39</b>	<b>50.92</b>	<b>77.34</b>	<b>43.77</b>	<b>72.68</b>	<b>46.53</b>	<b>74.42</b>	<b>46.55</b>	74.48

**Table 1. Summary: final semantic segmentation accuracy.** Unsupervised depth as pre-training improves semantic segmentation accuracy under all settings. Our best practice (in **blue**) improves common practice (in **red**) by 7.53% mIoU and 4.68% pixel accuracy. **Green**: results worse than random initialization. None: random initialization; ImageNet: ImageNet pre-trained; depth: depth pre-trained from scratch; depth-IN: depth pre-trained with ImageNet initialization. DeepLabV3<sup>†</sup>: with ResNet50 encoder.

optimizing a linear combination of photometric reprojection error and an edge-aware local smoothness prior

$$L(w') = w_{ph}\ell_{ph} + w_{sm}\ell_{sm}, \quad (13)$$

where

$$\ell_{ph} = \sum_{i,j,n,t} (1 - \text{SSIM}(x_{t+1}^n(i,j), \hat{x}_t^n(i,j))) + \alpha |x_{t+1}^n(i,j) - \hat{x}_t^n(i,j)|_1 \quad (14)$$

$\hat{x}_t$  is the warped image (see (1) for the definition);  $\ell_{sm}$  is the edge-aware smoothness prior

$$\ell_{sm} = \sum_{i,j,n,t} |\partial_X z_t^n(i,j)| e^{-|\partial_X x_t^n(i,j)|} + |\partial_Y z_t^n(i,j)| e^{-|\partial_Y x_t^n(i,j)|}, \quad (15)$$

$w_{ph}$  and  $w_{sm}$  are weights.

For semantic segmentation, we replace the last layer of the decoder by a fully connected layer. Monodepth2 has multi-scale output, we only use the finest scale output for semantic segmentation. All segmentation models are trained by cross-entropy loss with ADAM optimizer for 20000 iterations with cosine learning rate schedule. More implementation details are in the Appendix A

## 4.2 Results and Analysis on KITTI Dataset

We choose KITTI as our dataset, which contains 93000 dash-cam videos at 10 FPS for unsupervised pre-train, and has 200 annotated images for semantic segmentation fine-tune and evaluation, which allows us to perform unsupervised pre-training in the domain of interest. Semantic segmentation accuracy is evaluated by mean IoU across semantic classes (mIoU) and percentage of correctly labeled pixels (pixel accuracy). In the experiments we by default set image resolution to be 640×192 following the resolution used by Monodepth2. We also provide experimental results on a higher resolution, and discussions regarding robustness to resolutions

To better control variables in the experiments, we limit data augmentation to horizontal flip. We by default use a fixed subset of 16 randomly chosen images as the training set, and use the rest of the 184 images as validation set. We intentionally choose a small training set to better test the impact of pre-training. Nevertheless, we report results on different training-testing partitions in Fig. 4.

We adopt standard ResNet18 and ResNet50 backbones as encoder. This allows us to directly use PyTorch ImageNet pre-trained weights, and the backbones are compatible with other architectures (e.g. DeepLab V3). One trial on either ResNet 18 or ResNet50 takes around 2.5 hours. To report results, we run four independent trials for each setting and report the average. KITTI contains 21 semantic classes by default. We train on all 21 classes during the semantic fine-tuning. However, since we do not consider using a separate external dataset with segmentation labels, many of the semantic classes are rarely visible in the dataset (e.g. ‘train’, ‘motorcycle’), especially in the experiments where we fine-tune the network on only 16 images. In such cases,

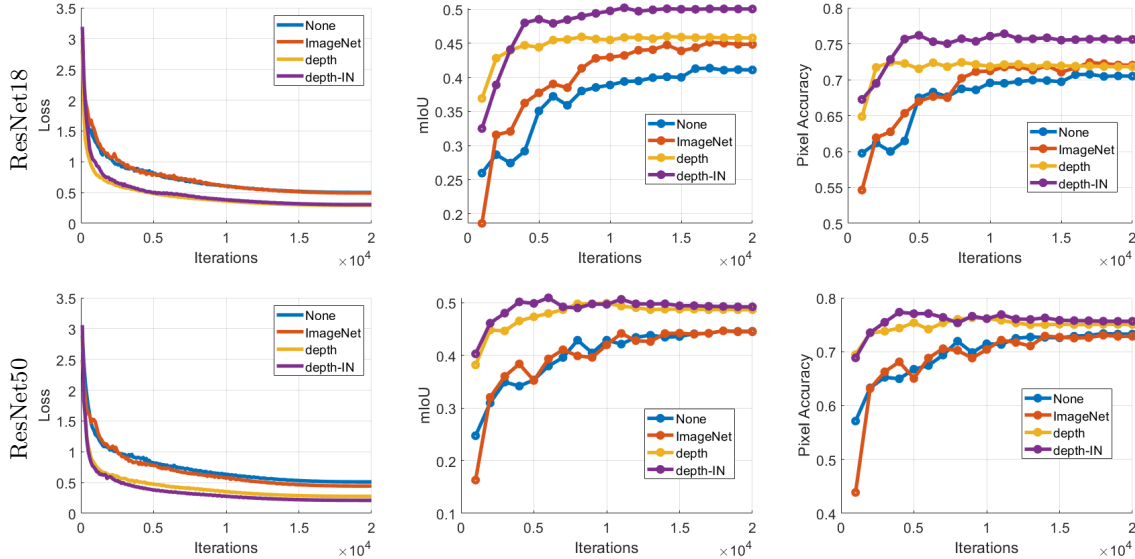


**Fig. 3. Comparison between different network initializations.** Models initialized by unsupervised depth pre-training train faster and achieve higher final accuracy.

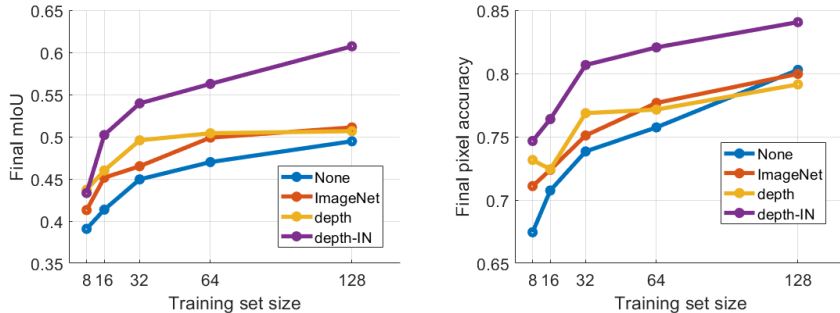
these classes always receive zero IoU, which pulls down the mIoU metric (but still yields high pixel accuracy). In Sect. 4.2, we compute mIoU on a subset of 7 representative classes unless further specified. Nevertheless, the results on 21 classes show exactly the same trends.

Fig. 2 summarizes our experimental setups. We test under different settings, including 1) fine-tune whole network; 2) fix pre-trained encoder, fine-tune decoder; 3) transfer pre-trained encoder to a different network architecture. Tab. 1 summarizes final results under different experimental settings. All results are computed by averaging 4 independent trials. Under all settings, unsupervised depth prediction improves semantic segmentation accuracy. Our best practice (ImageNet initialized depth as pre-train) improves common practice (ImageNet pre-train + DeepLab V3 head) by 7.53% on mIoU and 4.68% on pixel accuracy. We provide detailed analysis of the results below.

**Full model.** Fig. 3 shows the evolution of training loss and model accuracy. On both ResNet 18 and ResNet 50, depth pre-training outperforms ImageNet and random initialization. ImageNet pre-training slightly improves over random initialization on ResNet18, but shows almost identical performance to random initialization on ResNet50. Note that ours is more than  $3\times$  faster to train, around 5000 iterations, while ImageNet takes 15000 to 20000 iterations.

**Different training set size.** Fig. 3 summarizes final semantic segmentation accuracy varying the size of training set. All pre-training methods outperform random initialization when training samples are limited. When training samples increase (e.g 128), ImageNet pre-training and depth pre-training perform similarly to random initialization, but depth initialized by ImageNet still outperforms other methods.

**Frozen encoder.** We freeze pre-trained encoders, and fine-tune the decoder on semantic segmentation. This evaluates how well features from pre-trained encoders can predict semantics. In Figure 5, we present the training loss (left) and test accuracy (center, right) curves for the experiment. With both ResNet18 and ResNet50, using the fixed encoder pre-trained by depth significantly outperforms random initialization and ImageNet classification initialization. It is surprising that ImageNet pre-training is detrimental in this case – pre-training on ImageNet and fixing the encoder during fine-tuning performs worse than fixed random



**Fig. 4. Final accuracy vs different training set size.** Under all training set sizes, our best practice constantly outperforms ImageNet pre-trained. Encoder: ResNet18.

	ResNet18		ResNet50	
	mIoU	P.Acc	mIoU	P.acc
None	41.35	70.75	44.66	73.37
ImageNet	45.15	72.39	44.65	73.06
Depth (encoder only)	46.69	75.04	46.99	73.57
Depth (full)	50.20	76.39	50.92	77.34

**Table 2. Initializing with depth encoder and random decoder.** The depth network contains weights for both encoder and decoder. Depth (encoder only) initializes only the encoder of the semantic segmentation network with the depth encoder. Depth (full) initializes all the weights in the segmentation network with the exception of the prediction head (last layer). Initializing with just the encoder still outperforms initialization with ImageNet weights. Initializing with both encoder and decoder from depth network (the proposed method) performs the best.

weights.<sup>1</sup> We conjecture that uncontrolled biases in ImageNet and the task gap between classification and semantic segmentation cause difficulties in directly predicting segmentation without fine-tuning. ImageNet pre-training tends to favor generic texture features, that do not capture object shape, which makes fine-tuning the decoder difficult for learning segmentation.

**Neural Activation.** To gain more insights, we visualize the activations of the ResNet18 encoder by Grad-CAM [28]. Grad-CAM is originally designed for classification, we modify it for semantic segmentation by inspecting the gradient of neural response with respect to the summation of predicted labels for pixels instead of one single class label for the image. We choose to visualize shallow layers (before down pooling) for high spatial resolution. Fig. 4.2 shows two examples. Both our neural activation maps and segmentation outputs align with semantic boundaries. This confirms studies on image and range statistics discussed in prior work.

**Initializing with depth encoder and random decoder.** To eliminate the effect of the depth-initialized decoder and only test the encoder, we replace the pre-trained decoder by a ‘fresh’ randomly initialized decoder and fine-tune the whole network on semantic segmentation. The results are presented in Table 2 (marked blue). Initializing the encoder only by depth still outperforms ImageNet initialization, while initializing both encoder and decoder by depth performs the best. This shows that the final accuracy benefits from both the encoder and the decoder initialized by depth estimation.

**Higher resolutions and training on the full dataset.** In Figure 7 we show results trained on a higher image resolution (1024×320). We also provide results when trained on the full dataset (200 images), in which case we also train for an extended number of iterations (50000). Here we report the accuracy on the whole

<sup>1</sup> We performed a grid search for optimal learning rate for ImageNet pre-training.

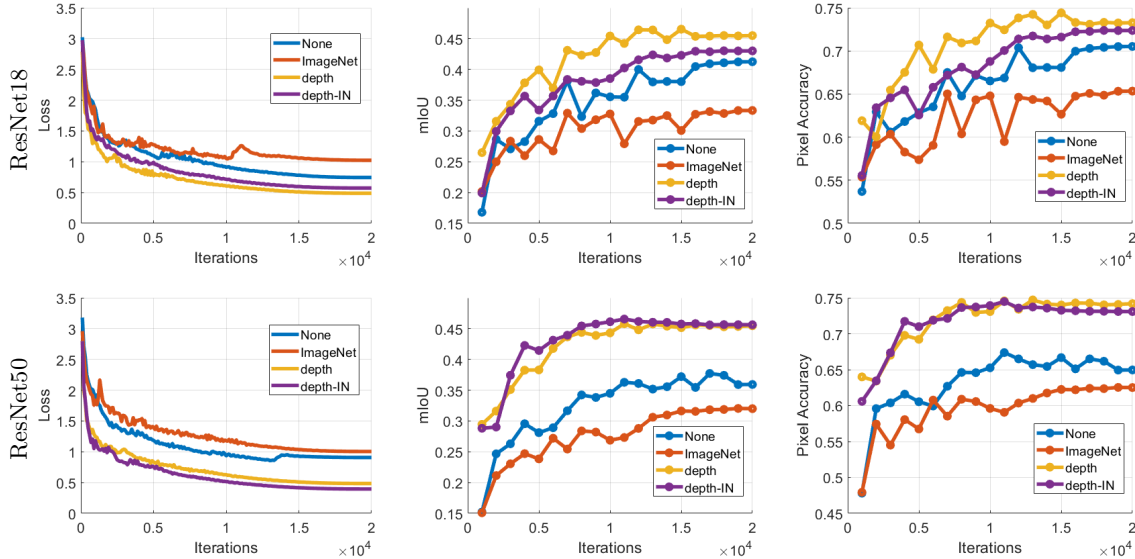


**Fig. 5. Frozen encoder results.** Using an encoder that was pre-trained by depth significantly outperforms one with random weights and ImageNet classification pre-trained weights. Note that in this experiment, ImageNet pre-training performs worse than random initialization.

dataset. As expected, segmentation accuracy improves significantly from the low resolution and small training set settings. Pre-training by depth still outperforms ImageNet pre-training and random initialization. Note that in this case using random initialization is unstable and training diverges after 30000 iterations.

**Cross Architecture.** To test whether the improvement is due to depth pre-trained encoders that favor our particular network architecture, we use pre-trained ResNet50 encoders to initialize DeepLab V3 and follow the same training procedure as common practice, which uses ImageNet initialization. Under this setting, All pre-trainings significantly improve accuracy compared with random initialization (Tab. 1). Our depth model trained from scratch can provide the same level of performance as ImageNet pre-training, while using ImageNet initialized depth slightly improves over ImageNet.

We also conduct the experiments on high resolution images. Results are consistent with low-resolution experiments. Although both ImageNet and depth initialization converged to a same level of accuracy, the depth pre-trained model shows a high accuracy in earlier iterations. This is interesting given that training loss of both ImageNet and depth pre-train are almost the same. We conjecture that the features learned by single-image depth estimation are more conducive to segmenting ‘bigger’ classes (e.g. ‘road’, ‘building’) which are mostly rigid and take up larger portions of the image.

To further investigate this behavior, in Figure 9 we plot the mIoU curve on all (21 classes), and a scatter plot of mIoU versus pixel accuracy in the training process. While mIoU on all 21 classes follow the trend observe on 7 classes, the scatter plot shows that at each same level of mIoU, models pre-trained by depth have higher pixel accuracy. This validates our conjecture that the depth-pre-trained model learns ‘bigger’ classes faster, since higher performance on these classes will result in high pixel accuracy as they have more pixels.

**Pre-training on depth is robust to different object scales.** Classification datasets tend to assign the label by a ‘primary’ object, and typical classification models are trained on fixed image resolution. Therefore, objects of interest tend to have a similar scale. For example, ImageNet models are by default trained on images resized to  $224 \times 224$  pixels, thus cars in the dataset typically have a size of 100 to 200 pixels. In

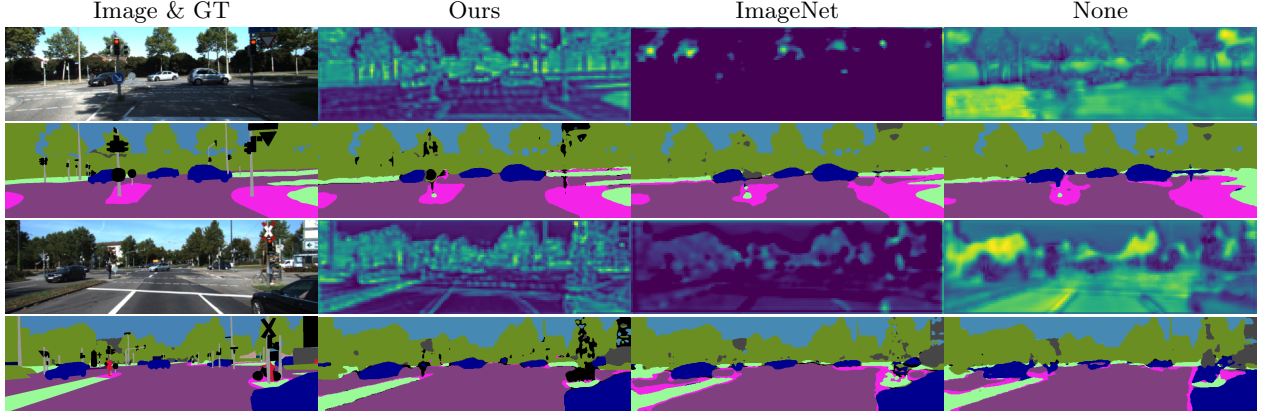


**Fig. 6. Neural activation and semantic segmentation result.** We visualize the neural activation map for a shallow layer of ResNet 18 encoder trained from different initializations, and their corresponding segmentation results. Boundaries are better aligned to semantic boundaries in our model. Note that only 16 annotated training samples are used to train the model. Better viewed zoomed-in.

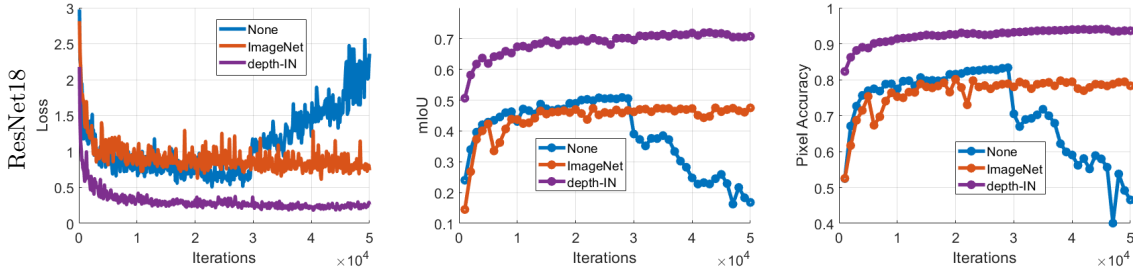


**Fig. 7. Training ResNet with high resolution images.** Similar to low resolution images, pre-training on depth also improves semantic segmentation accuracy on high resolution images.

semantic segmentation, however, objects may appear at different scales. The size of a car may vary from a few to a few thousand pixels. Even with manually added data augmentation, ImageNet pre-training does not cover such a wide range of scales.

Figure 10 illustrates the mismatch between cars in ImageNet and cars in KITTI. On the other hand, we conjecture that pre-training on depth improves robustness to different object scales. To validate this conjecture, we perform cross-resolution fine-tuning: depth pre-training on a smaller resolution, testing on a larger resolution; and pre-training on a larger resolution, testing on a smaller resolution. Since models pre-trained on larger resolution have ‘seen’ smaller scales (yellow box in Figure 10), they should still work on smaller images; on the other hand, models pre-trained on smaller resolution images have not seen objects of a larger scale (regions outside the yellow box), they should work poorly on larger images. Our experimental results validate conjecture: the former diverges during training in multiple independent trials while the latter achieves a final mIoU of 48.54 (ImageNet: 45.15, random: 41.35).

**Optical flow as pre-training.** We test whether pre-training by optical flow, which also minimizes photometric error with spatial regularity similar to monocular depth, one can achieve the same level of improvement in semantic segmentation. We train a siamese network with two shared-weight ResNet18 image encoders and one flow decoder, and use the encoder to initialize the semantic segmentation network. Details for training optical flow are in the Appendix B. Fig. 11 shows the result. While both optical flow and depth estimation output reasonable results and capture object boundaries, unlike depth, pre-training on optical flow is



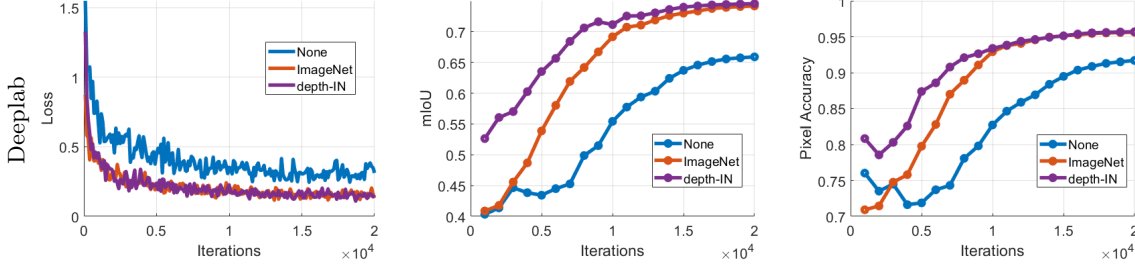


**Fig. 8. Training Deeplab on high resolution images.** Compared to lower resolutions, performance improves for different initializations. Training loss (left) is similar between ImageNet and depth initialization, but mIoU (center) and pixel accuracy (right) are higher for depth initialization for similar loss values.

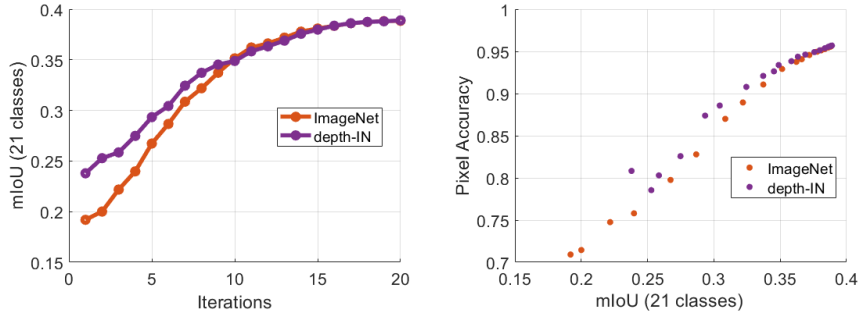


**Fig. 9. mIoU v.s. pixel accuracy during training DeepLab.** at each same level of mIoU, model pre-trained by depth has a higher pixel accuracy. This validates our conjecture that the depth-pre-trained model learns ‘bigger’ classes faster.

detrimental. We conjecture that flow does not require learning priors of the underlying 3-D scene. It can be estimated as long as features are discriminative and can support correspondence. On the contrary, depth estimation from a single image forces the network to learn priors on the scene, which can improve semantic segmentation.

### 4.3 Results on NYU-V2 Dataset

The NYU-V2 semantic segmentation dataset contains 795 densely annotated images for training and 654 for testing. Along with the training and testing set, there are also 407024 unannotated frames available, each comes with pairing depth image captured by depth camera. Since our claims are agnostic to how depth estimation models are trained (Sect. 2), we train monocular depth estimation directly on these image-depth pairs. Similar to the experiments on KITTI, we adopt Monodepth2, and test on both ResNet18 and ResNet50 encoders.

**Details for training on NYU-V2** Because NYU-V2 provide image and depth map pairs, we directly train Monodepth2  $\phi_w$  by minimizing an  $L_1$  loss:

$$\mathcal{L}_{L_1} = \sum_{n,i,j} \mathbb{1}(z^n(i,j) > 0) (|\phi_w(x^n)(i,j) - z^n(i,j)|), \quad (16)$$

where  $\phi_w(x)$  is the predicted depth for an image  $x$  and  $z$  is the ground truth depth from a Microsoft Kinect. Because the ground truth is only semi-dense, this loss is only computed where there is valid depth measurements *i.e.*,  $z(i,j) > 0$ .





**Fig. 10. Mismatch between object scales in ImageNet and KITTI.** ImageNet models are trained with a fixed input size and objects of interest tend to have a similar scale. However, objects in semantic segmentation dataset vary drastically in scales. Pre-training on depth provides robustness to scale change.



**Fig. 11. Depth helps, flow hurts.** While both are trained to minimize photometric reconstruction error, initializing from the network trained for single image depth prediction outperforms the one for flow. This stems from the fact that a single image does not support the inference of depth so the network must learn a rich prior over the structures within a scene. In contrast, flow does not require learning i.e. any discriminative features will support the correspondence search, so the pre-trained flow network is not constrained to learning properties of the scene.

We trained Monodepth2 using the ADAM optimizer with  $\beta_1 = 0.9$  and  $\beta_2 = 0.999$ . We set the initial learning rate to be  $1 \times 10^{-4}$  for 5 epochs and decreased it to  $5 \times 10^{-5}$  another 5 epochs for a total of 10 epochs. We used a batch size of 8 and resized each image to  $448 \times 384$ . For data augmentation, we perform random brightness, contrast and saturation adjustments within the range of  $[0.80, 1.20]$  with a 50% probability. Pre-training the depth network takes  $\approx 19$  hours for ResNet18 backbone and  $\approx 30$  hours for ResNet50. After pre-training, we do semantic segmentation fine-tuning on the training set. As with KITTI, we apply the ADAM optimizer with  $1 \times 10^{-5}$  initial learning rate and cosine learning rate decay, and restrict data augmentation to horizontal flipping. Limited by GPU memory, for ResNet18 we use batch size 32, and for ResNet50 we use batch size 16. All models are trained for 20000 iterations. Each experiment is repeated by four independent trials.

**Results** Figure 12 shows that, as with KITTI, initializing the model with depth pre-trained weights significantly improves semantic segmentation accuracy with both ResNet18 and ResNet50 encoders. Initializing by ImageNet pre-trained weights also improves from random initialization. Note that, with both encoders, pre-training by depth trains faster, which matches with our observations on KITTI. This may be due to that depth provides a pre-trained decoder, while for ImageNet pre-train, the decoder needs to be randomly initialized.

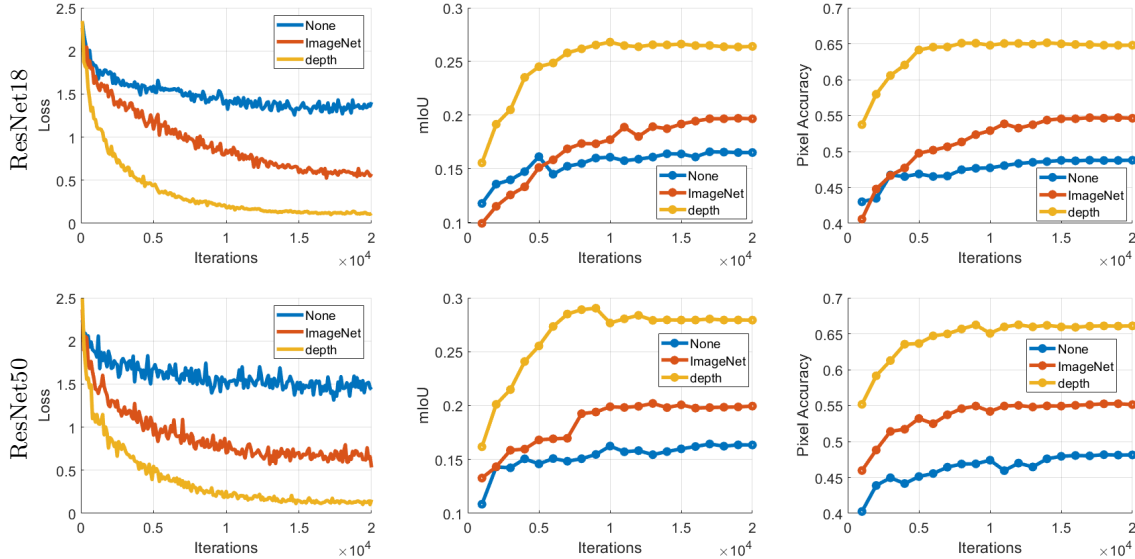


**Fig. 12. Results on NYU-V2.** Similar to KITTI, initializing the model with depth pre-trained weights trains faster and significantly improves semantic segmentation accuracy.

## 5 Discussion

In this paper we take issue with the widespread practice of using image classification as a pre-training task for a multitude of downstream tasks, such as semantic segmentation. The main problem is that image classification is *defined* by induction and therefore does not only entail, but *requires* a strong inductive bias, which opens the door to potentially pernicious side-effects. Induction is required because, continuing the example of the image labeled as “cow”, there is nothing in the image of a scene that would enable one to infer the three-letter word “cow.” The only reason we can do so is because the present image resembles, in some way implicitly defined by the training process, *different images, of different scenes*, that some human has tagged with the word “cow.” However, since images, no matter how many, are infinitely simpler than even a single scene, say the present one, this process is not forced to learn that the extant world even exists. Rather, it learns regularities in images, each of a different scene since current models are trained with data aiming to be as independent as possible, agnostic of the underlying scene.

Conversely, depth estimation, which requires multiple images *of the same underlying scene*, does not require inductive bias beyond a basic image-formation model of the form (1) to relate the geometry of the scene  $z$  to the disparity of images  $x_{t+1}, \hat{x}_t$ . While depth estimation *may benefit* from induction, for instance to sharpen the priors in non-informative regions (the Aperture Problem), it does not require it [22].

Now, one may object that monocular depth estimation is itself undecidable. This is why monocular depth estimators are trained with either multiple views (motion or stereo), or with some form of supervision or partial backing from additional modalities, such as sparse depth from lidar [24] or other range sensor [29]. Then, a depth estimate is just a statistic of the learned prior. As a result, depth estimation networks should never produce *one* depth estimate for each image, but rather a distribution over depth maps, conditioned on the given image [43,44]. Given an image, every depth map is possible, but they are not equally likely. The posterior over depth given an image then acts as a prior in depth inference using another modality, *e.g.*, unsupervised depth completion. The mode of this conditional prior can then be used as a depth estimate if one so desires, but with the proviso that whatever confidence one may place in that point estimate comes from inductive biases that cannot be validated.

One additional objection is that, since depth requires optimization to be inferred, and the choice of loss function is a form of transductive bias, that is no less arbitrary than inductive bias. But this is fundamentally

not the case, for the optimization residual in transductive inference refers to the data *here and now*, and not to data of different images in different scenes. In other words, the optimization residual is informative of the confidence of our estimate, unlike the discriminant from an inductively-trained classifier [11].

Another objection is that, if the optimization is performed relative to the re-projection error, then re-projection – if performed causally in time – can be understood as a form of prediction, and many approaches have used prediction as a generic task for pre-training models. This is true, but with two caveats: First, predicting the next image without additional modeling assumptions does not require assuming that there is an underlying 3-D scene, just that there is an unstructured displacement field that can move pixels from one image to the next. Only if this displacement field, or its diffeomorphic closure, has the structure of an epipolar transformation [31], can we conclude that the prediction task is forced to “understand” the scene, meaning that the hypothesis space is in the space of scenes (depth maps) not image displacements, that again do not require the existence of the scene. Second, video prediction – while promising – has not yet panned out as a generic pre-training task, despite many attempts [21,40,13,36]. This may be due to the fact that prediction of the pixels “per-se” does not force the model to infer anything about the scene, which is a necessary step for effective pre-training of visual inference engines.

In this paper, we aim to bypass the artificial constraints imposed both by supervised classification, and self-supervision. Instead, we simply use videos to pre-train a model for depth estimation, without supervision. Then, one can use supervision to fine-tune the model for semantic segmentation. These two tasks are seemingly antipodal, yet depth estimation outperforms image classification when used as pre-training for semantic segmentation.

This also addresses one last objection that one can move to our thesis, that is that, since ImageNet data is available, it makes sense to use it. What we argue here is that, actually, it does not. The argument is corroborated by evidence: Pre-training on a geometric task improves fine-tuning a semantic task, even when compared with pre-training with a different semantic task. Nonetheless, ImageNet pre-training can be useful to expedite training depth estimation networks, likely due to the formation of generic filter banks in the early layers.

**Limitations.** Our method possesses several limitations. The first is that it requires use of a calibrated camera. Therefore, one cannot use generic videos harvested from the web. There is nothing that in principle prevents us from using uncalibrated cameras, simply by adding the calibration matrix  $K$  to the nuisance variables. While the necessary conditions for full Euclidean reconstruction are rarely satisfied in consumer videos (for instance, they require cyclorotation around the optical axis, not just panning and tilting), the degrees of freedom that cannot be reconstructed are moot as they do not affect the reprojection. Extension to uncalibrated cameras is part of future research.

Even if the camera is calibrated, rigid motion is only defined if the underlying scene is rigid. If independently moving objects occupy a small portion of the visual field, they will be rejected as outliers, but the method cannot work with swarms of bees and other amorphous scene dynamics. This is fundamental, but can be overcome by stereo, where multiple images are captured from different vantage points at the same time, so the scene appears rigid in the instant.

Another limitation is the use of relatively few datasets for empirical validation. While the motivation of this work is to use data that is not annotated for pre-training, we do require detailed annotation for validation and experimental comparison, and there are not many datasets from which we can sequester a reasonable held-out fraction for validation and testing. For this reason, we have limited the size of the fine-tuning set, so as to leave the largest possible calibration set. Extending the evaluation to larger datasets will likely require use of synthetic data. However, at present synthetic data still includes significant enough artifacts to thwart successful pre-training of depth estimation for semantic segmentation.

## References

1. Achille, A., Lam, M., Tewari, R., Ravichandran, A., Maji, S., Fowlkes, C.C., Soatto, S., Perona, P.: Task2vec: Task embedding for meta-learning. In: Proceedings of the IEEE/CVF International Conference on Computer Vision. pp. 6430–6439 (2019)
2. Achille, A., Paolini, G., Soatto, S.: Where is the information in a deep neural network? arXiv preprint arXiv:1905.12213 (2019)
3. Achille, A., Soatto, S.: Emergence of invariance and disentanglement in deep representations. *The Journal of Machine Learning Research* **19**(1), 1947–1980 (2018)
4. Brown, T., Mann, B., Ryder, N., Subbiah, M., Kaplan, J.D., Dhariwal, P., Neelakantan, A., Shyam, P., Sastry, G., Askell, A., et al.: Language models are few-shot learners. *Advances in neural information processing systems* **33**, 1877–1901 (2020)
5. Caron, M., Bojanowski, P., Mairal, J., Joulin, A.: Unsupervised pre-training of image features on non-curved data. In: Proceedings of the IEEE/CVF International Conference on Computer Vision (ICCV) (October 2019)
6. Chaudhari, P., Soatto, S.: Stochastic gradient descent performs variational inference, converges to limit cycles for deep networks. In: 2018 Information Theory and Applications Workshop (ITA). pp. 1–10. IEEE (2018)
7. Chen, L.C., Papandreou, G., Kokkinos, I., Murphy, K., Yuille, A.L.: Deeplab: Semantic image segmentation with deep convolutional nets, atrous convolution, and fully connected crfs. *IEEE transactions on pattern analysis and machine intelligence* **40**(4), 834–848 (2017)
8. Chen, M., Artières, T., Denoyer, L.: Unsupervised object segmentation by redrawing. *Advances in neural information processing systems* **32** (2019)
9. Chen, T., Kornblith, S., Norouzi, M., Hinton, G.: A simple framework for contrastive learning of visual representations. In: International conference on machine learning. pp. 1597–1607. PMLR (2020)
10. Chen, X., Fan, H., Girshick, R., He, K.: Improved baselines with momentum contrastive learning. arXiv preprint arXiv:2003.04297 (2020)
11. Der Kiureghian, A., Ditlevsen, O.: Aleatory or epistemic? does it matter? *Structural safety* **31**(2), 105–112 (2009)
12. Godard, C., Mac Aodha, O., Firman, M., Brostow, G.J.: Digging into self-supervised monocular depth prediction (October 2019)
13. Guen, V.L., Thome, N.: Disentangling physical dynamics from unknown factors for unsupervised video prediction. In: Proceedings of the IEEE/CVF Conference on Computer Vision and Pattern Recognition. pp. 11474–11484 (2020)
14. He, K., Girshick, R., Dollár, P.: Rethinking imagenet pre-training. In: Proceedings of the IEEE/CVF International Conference on Computer Vision. pp. 4918–4927 (2019)
15. Hoffman, J., Tzeng, E., Park, T., Zhu, J.Y., Isola, P., Saenko, K., Efros, A., Darrell, T.: Cycada: Cycle-consistent adversarial domain adaptation. In: International conference on machine learning. pp. 1989–1998. PMLR (2018)
16. Hoyer, L., Dai, D., Chen, Y., Köring, A., Saha, S., Van Gool, L.: Three ways to improve semantic segmentation with self-supervised depth estimation. In: Proceedings of the IEEE/CVF Conference on Computer Vision and Pattern Recognition (CVPR). pp. 11130–11140 (2021)
17. Hoyer, L., Dai, D., Wang, Q., Chen, Y., Van Gool, L.: Improving semi-supervised and domain-adaptive semantic segmentation with self-supervised depth estimation. arXiv preprint arXiv:2108.12545 [cs] (2021)
18. Huang, J., Lee, A.B., Mumford, D.: Statistics of range images. In: Proceedings IEEE Conference on Computer Vision and Pattern Recognition. CVPR 2000 (Cat. No. PR00662). vol. 1, pp. 324–331. IEEE (2000)
19. Huang, J., Mumford, D.: Statistics of natural images and models. In: Proceedings. 1999 IEEE Computer Society Conference on Computer Vision and Pattern Recognition (Cat. No PR00149). vol. 1, pp. 541–547. IEEE (1999)
20. Huang, S., Lu, Z., Cheng, R., He, C.: Fapn: Feature-aligned pyramid network for dense image prediction. In: Proceedings of the IEEE/CVF International Conference on Computer Vision. pp. 864–873 (2021)
21. Jin, B., Hu, Y., Tang, Q., Niu, J., Shi, Z., Han, Y., Li, X.: Exploring spatial-temporal multi-frequency analysis for high-fidelity and temporal-consistency video prediction. In: Proceedings of the IEEE/CVF Conference on Computer Vision and Pattern Recognition. pp. 4554–4563 (2020)
22. Julesz, B.: Binocular depth perception without familiarity cues: Random-dot stereo images with controlled spatial and temporal properties clarify problems in stereopsis. *Science* **145**(3630), 356–362 (1964)
23. Julesz, B.: Foundations of cyclopean perception. (1971)
24. Kuznetsov, Y., Stuckler, J., Leibe, B.: Semi-supervised deep learning for monocular depth map prediction. In: Proceedings of the IEEE conference on computer vision and pattern recognition. pp. 6647–6655 (2017)
25. Li, X., You, A., Zhu, Z., Zhao, H., Yang, M., Yang, K., Tan, S., Tong, Y.: Semantic flow for fast and accurate scene parsing. In: European Conference on Computer Vision. pp. 775–793. Springer (2020)

26. Lopez-Rodriguez, A., Busam, B., Mikolajczyk, K.: Project to adapt: Domain adaptation for depth completion from noisy and sparse sensor data. In: *Proceedings of the Asian Conference on Computer Vision* (2020)
27. Lowe, D.G.: Distinctive image features from scale-invariant keypoints. *International journal of computer vision* **60**(2), 91–110 (2004)
28. Selvaraju, R.R., Cogswell, M., Das, A., Vedantam, R., Parikh, D., Batra, D.: Grad-cam: Visual explanations from deep networks via gradient-based localization. In: *Proceedings of the IEEE international conference on computer vision*. pp. 618–626 (2017)
29. Smisek, J., Jancosek, M., Pajdla, T.: 3d with kinect. In: *Consumer depth cameras for computer vision*, pp. 3–25. Springer (2013)
30. Soatto, S., Chiuso, A.: Visual representations: Defining properties and deep approximations. *arXiv preprint arXiv:1411.7676* (2014)
31. Sundaramoorthi, G., Petersen, P., Varadarajan, V., Soatto, S.: On the set of images modulo viewpoint and contrast changes. In: *2009 IEEE Conference on Computer Vision and Pattern Recognition*. pp. 832–839. IEEE (2009)
32. Tishby, N., Pereira, F.C., Bialek, W.: The information bottleneck method. *arXiv preprint physics/0004057* (2000)
33. Tsai, Y.H., Hung, W.C., Schuster, S., Sohn, K., Yang, M.H., Chandraker, M.: Learning to adapt structured output space for semantic segmentation. In: *Proceedings of the IEEE conference on computer vision and pattern recognition*. pp. 7472–7481 (2018)
34. Tsai, Y.H., Sohn, K., Schuster, S., Chandraker, M.: Domain adaptation for structured output via discriminative patch representations. In: *Proceedings of the IEEE/CVF International Conference on Computer Vision*. pp. 1456–1465 (2019)
35. Van Gansbeke, W., Vandenhende, S., Georgoulis, S., Van Gool, L.: Unsupervised semantic segmentation by contrasting object mask proposals. In: *Proceedings of the IEEE/CVF International Conference on Computer Vision*. pp. 10052–10062 (2021)
36. Wang, Y., Wu, J., Long, M., Tenenbaum, J.B.: Probabilistic video prediction from noisy data with a posterior confidence. In: *Proceedings of the IEEE/CVF Conference on Computer Vision and Pattern Recognition*. pp. 10830–10839 (2020)
37. Wong, A., Cicek, S., Soatto, S.: Learning topology from synthetic data for unsupervised depth completion. *IEEE Robotics and Automation Letters* **6**(2), 1495–1502 (2021)
38. Wong, A., Fei, X., Tsuei, S., Soatto, S.: Unsupervised depth completion from visual inertial odometry. *IEEE Robotics and Automation Letters* **5**(2), 1899–1906 (2020)
39. Wong, A., Soatto, S.: Unsupervised depth completion with calibrated backprojection layers. In: *Proceedings of the IEEE/CVF International Conference on Computer Vision*. pp. 12747–12756 (2021)
40. Wu, Y., Gao, R., Park, J., Chen, Q.: Future video synthesis with object motion prediction. In: *Proceedings of the IEEE/CVF Conference on Computer Vision and Pattern Recognition*. pp. 5539–5548 (2020)
41. Yang, Y., Lao, D., Sundaramoorthi, G., Soatto, S.: Phase consistent ecological domain adaptation. In: *Proceedings of the IEEE/CVF Conference on Computer Vision and Pattern Recognition*. pp. 9011–9020 (2020)
42. Yang, Y., Loquercio, A., Scaramuzza, D., Soatto, S.: Unsupervised moving object detection via contextual information separation. In: *Proceedings of the IEEE/CVF Conference on Computer Vision and Pattern Recognition*. pp. 879–888 (2019)
43. Yang, Y., Soatto, S.: Conditional prior networks for optical flow. In: *Proceedings of the European Conference on Computer Vision (ECCV)*. pp. 271–287 (2018)
44. Yang, Y., Wong, A., Soatto, S.: Dense depth posterior (ddp) from single image and sparse range. In: *Proceedings of the IEEE/CVF Conference on Computer Vision and Pattern Recognition*. pp. 3353–3362 (2019)
45. Yun, S., Oh, S.J., Heo, B., Han, D., Choe, J., Chun, S.: Re-labeling imagenet: from single to multi-labels, from global to localized labels. In: *Proceedings of the IEEE/CVF Conference on Computer Vision and Pattern Recognition*. pp. 2340–2350 (2021)
46. Zamir, A.R., Sax, A., Shen, W., Guibas, L.J., Malik, J., Savarese, S.: Taskonomy: Disentangling task transfer learning. In: *Proceedings of the IEEE conference on computer vision and pattern recognition*. pp. 3712–3722 (2018)
47. Zhao, Y., Wang, G., Luo, C., Zeng, W., Zha, Z.J.: Self-supervised visual representations learning by contrastive mask prediction. In: *Proceedings of the IEEE/CVF International Conference on Computer Vision*. pp. 10160–10169 (2021)

## A Training and Evaluation Details

**Semantic segmentation fine-tuning.** Following the notation in Sect. 3.1, we denote with  $\phi_{w''} : \mathbf{x} \mapsto \hat{\mathbf{y}}$  the semantic segmentation network to be fine-tuned, which maps an image  $\mathbf{x}$  to a semantic label  $\mathbf{y}$ . Note that  $\phi_{w'}$  (classification network) is parameterized by weights  $w'$  of the ‘encoder’ network, and  $\phi_w$  (depth network) is parameterized by weights  $w$  of both the ‘encoder’ and a ‘decoder’. When pre-trained for classification, we initialize the encoder part of  $w''$  by  $w'$  and the decoder part by random weights; when pre-trained for depth, we initialize both encoder and decoder in  $w''$  using  $w$ , except for the last layer, where we change to a randomly initialized fully-connected layer with soft-max. During semantic segmentation fine-tuning, we update  $w''$  (see equation (11) and (12) in the main paper) by minimizing the cross entropy loss

$$L(w''|\bullet) = \sum_{i,j,n,k} -\log(\hat{y}^n(i,j))\mathbb{1}(y^n(i,j) = k) \quad (17)$$

where  $i, j$  are the pixel coordinates,  $n$  is the number of images in the training set,  $k$  is the class label,  $\hat{y} = \phi_{w''}(\mathbf{x}^n)$  is the network output. This is implemented via the Negative Log Likelihood (NLL) loss in Pytorch. Under different experimental settings, we either update all parameters in  $w''$  or only the decoder part of  $w''$  to minimize (17).

**Image normalization.** In fine-tuning, we apply the same image normalization that is consistent with the pre-training step. If the network is pre-trained by ImageNet classification, we normalize the image values by mean=[0.485, 0.456, 0.406], std=[0.229, 0.224, 0.225]; if pre-trained by Monodepth2, we normalize the image values to [0,1]; we also normalize to [0,1] when training from random initialization.

**Optimizer.** After a grid search, we choose  $1 \times 10^{-5}$  as the initial learning rate for the ADAM optimizer. The learning rate is updated by a standard cosine learning rate decay schedule in every iteration.

## B Details for training optical flow

To train a neural network  $f_\theta$  parameterized by  $\theta$  to estimate optical flow for a pair of images  $(x_t, x_{t+1})$  from time step  $t$  to  $t+1$ , we leverage the photometric reconstruction loss by minimizing a color consistency term and a structural consistency term (SSIM) between an image  $x_{t+1}$  and its reconstruction  $\hat{x}_t$  given by the warping  $x_t$  with the estimated flow  $f_\theta(x_t, x_{t+1})$ :

$$L_{ph} = \sum_{n,i,j,t} \lambda_{co}(|x_{t+1}^n(i,j) - \hat{x}_t^n(i,j)|) + \lambda_{st}(1 - SSIM(x_{t+1}^n(i,j), \hat{x}_t^n(i,j))), \quad (18)$$

where  $\hat{x}_t = x_t \circ f_\theta(x_t, x_{t+1})$ ,  $f_\theta(\cdot) \in \mathbb{R}^{2HW}$  and  $\lambda_{co} = 0.15$ ,  $\lambda_{st} = 0.15$  are the weights for color consistency and SSIM terms for  $L_{ph}$ , respectively.

Additionally, we minimize an edge-aware local smoothness regularizer:

$$L_{sm} = \lambda_{sm} \sum_{n,i,j} \lambda_X(i,j)|\partial_X f_\theta(x_t^n, x_{t+1}^n)(i,j)| + \lambda_Y(i,j)|\partial_Y f_\theta(x_t^n, x_{t+1}^n)(i,j)| \quad (19)$$

where  $\lambda_{sm} = 5$  is the weight of the smoothness loss,  $\partial_X, \partial_Y$  are gradients along the x and y directions, and the loss for each direction is weighted by  $\lambda_X := e^{-|\partial_X x_t^n|}$  and  $\lambda_Y := e^{-|\partial_Y x_t^n|}$  respectively.

We trained  $f_\theta$  using Adam optimizer with  $\beta_1 = 0.9$  and  $\beta_2 = 0.999$ . We set the initial learning rate to be  $5 \times 10^{-4}$  for the first 25 epochs and decreased it to  $5 \times 10^{-5}$  another 25 epochs. We used a batch size of 8 and resized each image to  $640 \times 192$ . Because KITTI has two video streams from left and right stereo camera, we randomly sample batches from each stream with a 50% probability. Training takes  $\approx 10$  hours for ResNet18 backbone and  $\approx 20$  hours for ResNet50.